Microwave Radiometric Observation of a Waterspout Over Coastal Arabian Sea

C. Suresh Raju, R. Renju, Tinu Antony, Nizy Mathew, and K. Krishna Moorthy

***Abstract*—This letter discusses the background thermodynamic conditions of a convective cloud during the occurrence of a waterspout. This study is conducted using a very unique experimental observation of a ground-based multifrequency microwave radiometer which was set to scan the atmosphere in seven elevation angles. The spatio-temporal variations of the cloud microphysical parameters during the evolution of a multicell convective cumulus system are studied. Humidity and temperature anomalies deduced from the radiometric observation could clearly explain the convective processes like the formation of an intense updraft of moist air, convective heating due to large latent heat energy release, and cooling of the lower atmosphere below 2-km altitude by the downdrafting dry air. The measurements from collocated IR radiometer, surface met sensors, and calculated CAPE showed the formation of an intense convection in a humid warm atmosphere over a shallow warm ocean (conducive to formation of a waterspout). Studies on the evolution of cloud parameters during the life cycle of convective precipitation are of great interest in weather forecasting.**

***Index Terms*—Convective system, microwave radiometer, waterspout.**

I. Introduction

SATELLITE-based microwave remote sensing is an effective tool for studying the spatial and vertical distribution of the atmospheric water vapor and temperature [1]. Remote sensing of air temperature and relative humidity (RH) in the lower atmosphere is of great interest in understanding the evolution of the boundary layer and convective systems. The ground-based radiometric profiling technique provides continuous measurements under a wide range of meteorological conditions [2], [3]. In contrast to satellite-based microwave remote sensing, having coarse spatial and temporal resolution, ground-based radiometric observations with very high temporal resolution are useful for studying localized convective events more effectively [4], [5].

Waterspouts are less intense than tornadoes, being a similar manifestation of small concentrated atmospheric vortices and commonly associated with cumulus clouds at 3–8 km altitudes [6]. Local convective events, which develop into cumulonimbus clouds in warm and moisture-laden environments, form the basis of waterspouts. Most of the studies reported on waterspouts are based on radar reflectivity and photography [7] and are from the mid-latitude regions. However, limited information is available on the cloud microphysics and thermodynamics associated with waterspouts [8]. Microwave radiometer observations of a waterspout can provide the microphysical information concerning the cloud system based on spatio-temporal variations of water vapor, liquid-water content, and thermal energy. This letter presents for the first time a report of multifrequency microwave radiometric observations of a tropical local convective cumulonimbus cloud system which led to the formation of a waterspout over the coastal Arabian Sea.

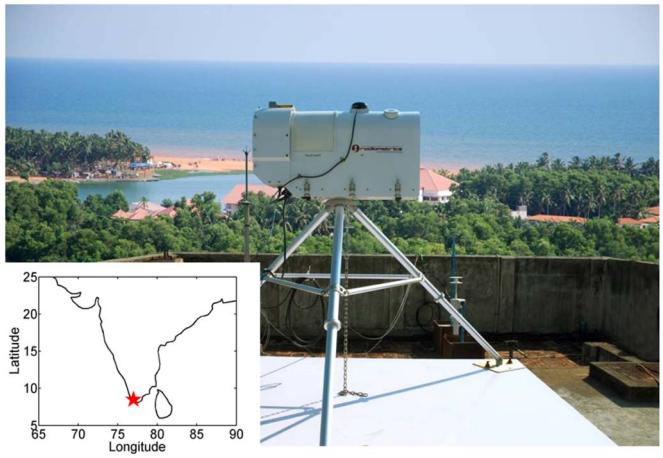

Fig. 1. Microwave radiometer site at the tropical coastal station Thiruvananthapuram. The system scans the atmosphere over land and sea during its elevation scan from 15° to 165°. The location of TVM is shown in the inset.

II. Site, Instrumentation, and Data

A ground-based hyperspectral microwave radiometer profiler (MRP) (model: Radiometrics 3000A www.radiometrics.com [9], [10]) has been operational at Space Physics Laboratory, VSSC, ISRO, Thiruvananthapuram (TVM), 8.55° N, 77° E (located on a hillock 75 m from the mean sea level), and ∼200 m inland from the Arabian Sea coast (Fig. 1). It measures radiometric brightness temperatures (T_B) through a sequential scan of five frequencies in the K-band (22–30 GHz) and seven in the V-band (51–59 GHz). The bandwidth for each channel is 300 MHz, with a beam width of 6° at 22–30 GHz and 3° at 51–59 GHz. The RH at each altitude is derived from the temperature and water-vapor measurements of the MRP. The radiometer also provides vertically integrated water vapor (IWV) and cloud liquid water (CLW). Meteorological sensors are attached to the radiometer to make *in situ* measurements of ambient temperature, pressure, and RH at the surface. A zenith-looking

Manuscript received November 11, 2011; revised September 12, 2012, October 17, 2012, and November 1, 2012; accepted November 19, 2012. The work of R. Renju and A. Tinu was supported by ISRO Research Fellowship.

The authors are with Space Physics Laboratory, Thiruvananthapuram 695022, India (e-mail: c_sureshraju@vssc.gov.in; renjusreeprasad@gmail.com; tinu_antony@vssc.gov.in; nizy_mathew@vssc.gov.in; krishnamoorthy_k@vssc.gov.in).

Color versions of one or more of the figures in this paper are available online at http://ieeexplore.ieee.org.

Digital Object Identifier 10.1109/LGRS.2012.2229960

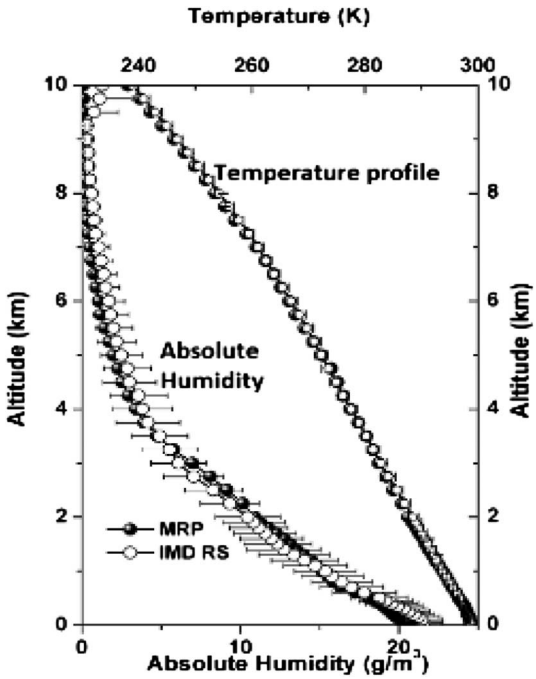

Fig. 2. Comparison of retrieved temperatures and absolute humidity profiles from MRP and IMD radiosonde (IMD RS) observations monthly averaged for the month of April 2011.

IR radiometer integrated to the MRP measures the cloud-base temperature for deducing the cloud-base height (CBH).

The vertical profiles of temperature and water vapor up to a height of 10 km are retrieved using a neural network technique (NN) from the microwave T_B measurements at different frequencies, IR temperature, and *in situ* met sensor measurements. The NN is trained for the tropical atmosphere using a series of historical radiosonde profile data from the India Meteorological Department (IMD) station at TVM [4]. There are several reports on the accuracy of profiler retrievals using hyperspectral radiometers based on direct comparison with simultaneous collocated radiosonde ascents [5] as well as postprocessed simulations using 1-D variational analysis under different meteorological conditions [11], [12]. The accuracies of retrieved temperature and water vapor under nonprecipitating conditions are summarized [13]. In the case of CLW retrievals, in nonprecipitating conditions, the error was found to be ∼15% [14].

MRP observations are commonly used to estimate temperature and moisture profiles by virtue of variation in weighting functions for different frequencies. The vertical resolution and accuracy of retrieved profiles decrease with increasing altitude. The NN method partially overcomes the lack of sensitivity at the higher levels by incorporating statistical correlations between lower and higher levels. The use of proper background data and vertical statistics is vital for achieving the highest accuracy [12]. The comparison of retrieved profiles of temperature and RH from MRP and the daily radiosonde profiles of IMD (from the nearest location, ∼5 km inland) for the month of April is shown in Fig. 2. The radiosonde measurements which are at definite pressure levels are interpolated according to the MRP altitude resolution, such as 50, 100, and 250 m in the altitude ranges of 0–500 m, 500 m–2 km, and 2–10 km. These temperature profiles show a good agreement with a mean absolute difference of < 0.5 K below 3 km and < 1 K above

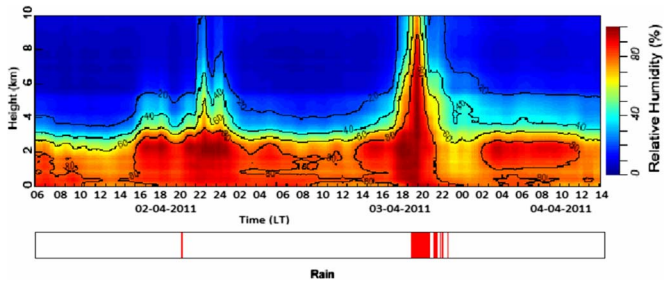

Fig. 3. Continuous evolution of RH (in percent) retrieved from the microwave radiometer observation from April 2 to 4, 2011, over sea. Rain flags are shown in vertical bars.

8 km. For absolute humidity, it is < 1.3 g $\cdot$ m^{-3} below 2 km. Similar results are reported by Cimini *et al.* [15].

III. Radiometric Observations of Waterspout

The microwave radiometer is aligned in the North–South direction, parallel to the coast line. An elevation scan along the orthogonal (East–West) direction enables the measurement of the microwave thermal emission from the atmosphere over the land and the sea. The radiometer is configured to scan at seven elevation angles of 15°, 30°, 45°, 90°, 135°, 150°, and 165°. For the first three elevation angles (15°, 30°, 45°), the radiometer scans the atmosphere over the land. At the last three angles (135°, 150°, 165°), it scans over the sea. The scan angle of 90° corresponds to the zenith. In this configuration, the profiles are obtained for each elevation angle at 3-min intervals.

Local convective systems form frequently over TVM during the summer season (March to May) due to the proximity to the equator. These systems can have genesis over land as well as over sea. Such a system, which led to the formation of a waterspout, was observed on April 3, 2011, and its evolution and propagation across the coast were observed using the MRP. Fig. 3 shows the temporal variation of RH observed using MRP over the sea for approximately 56 h, starting from 06:00 LT on April 2, 2011. While highly humid condition ($RH > 80\%$) existed below 3 km, dry conditions (RH $< 20\%$) prevailed above 5 km. Below 2 km, the absolute humidity was > 20 g $\cdot$ m^{-3}, and above 4 km, it was < 5 g $\cdot$ m^{-3}. The IWV during this period remained high at about 40–50 mm.

Over the tropics, severe convection tends to maximize in the late afternoon and evening hours, in response to the enhanced thermodynamic instability associated with diurnal heating. On April 2, at about 19:00 LT, the RH shows a rapid build up in its vertical distribution, which is an indicator for the development of local convection. On April 3, the event day, around 17:00 LT, strong and deep convection was observed, which pumped the humidity deep into the atmosphere beyond 10 km. This resulted in heavy precipitation for more than 1 h over the radiometer site (rain flag shown in red bars at the bottom of Fig. 3). Rain has an adverse effect on the retrieval of water vapor, temperature, and CLW. Rain-effect mitigation techniques used in the system (super blower and hydrophobic radome) minimize the error to a certain extent [16]. However, the liquid water on top of the radome that is not cleared by the blower can cause a relatively small increase in zenith T_B. Hence, we mainly rely on 15° elevation observations to substantially mitigate the impact of rain residual. Around 18:00 LT on this day, occurrence of a waterspout over the adjoining

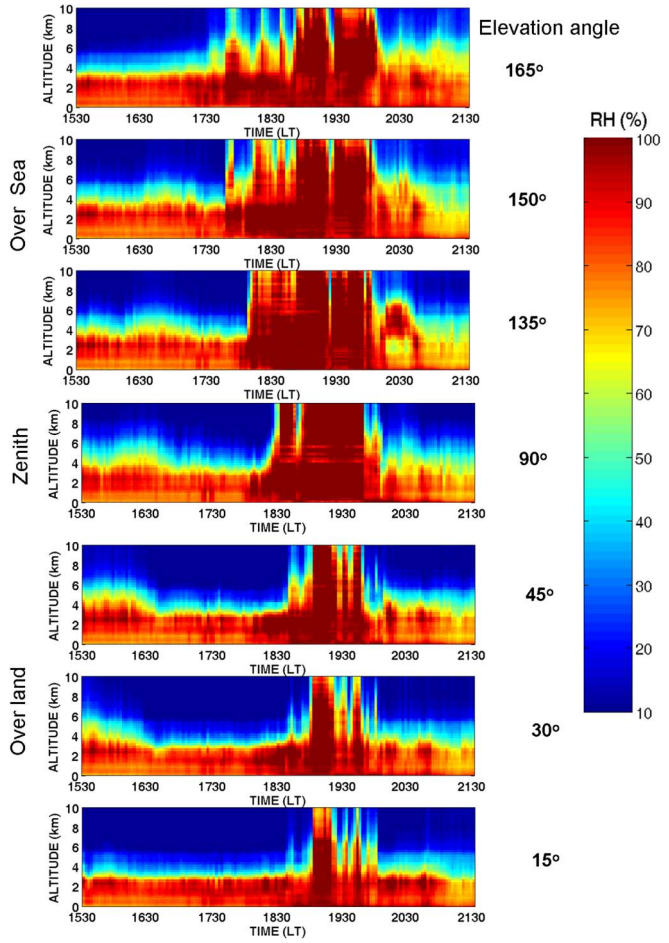

Fig. 4. Real-time evolution of the convective event on April 3, 2011, zoomed in for details. Panels 1 to 7 from the top correspond to the beams at 165°, 150°, 135°, 90°, 45°, 30°, and 15° elevation angles, respectively.

sea was clearly visible from the beach (∼500 m west of the radiometer site). This was reported in the local edition of the national daily (http://www.thehindu.com/todays-paper/tp-national/tp-kerala/article1598354.ece).

Fig. 4 shows the continuous evolution of the convective system in terms of RH variation, from its genesis to its gradual growth into a mature stage, followed by the abrupt dissipation, for the seven different elevation angles. The convection began over the sea around 17:30 LT (panel 1 from the top), and it persisted for around 3 h. Panels 2–4 show the gradual growth in intensity and the spatial extent of the system toward the coast. The system crossed the shore around 18:00 LT and entered the land (panels 5–7). From these figures, it is inferred that convection was initiated over the sea, and it became fully developed in terms of high humidity and liquid-water content by 19:00 LT and then spread and dissipated over land.

The temporal variation of T_B at 30 GHz is a direct indicator for the variations of CLW since the thermal emission from liquid water is more sensitive at 30 GHz. Fig. 5 shows the temporal variation of T_B at 30 GHz during the convection, with the first (from top) panel for elevation angles 165° (red) and 15° (blue), the second panel for 150° (red) and 30° (blue), and the third panel for 135° (red) and 45° (blue). In the top panel, the prevailing (background) T_B over the sea is ∼100 K (before the convection) which gradually increases to ∼300 K

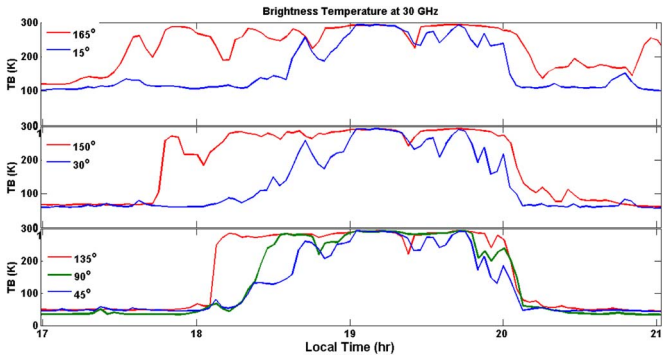

Fig. 5. Temporal variation of T_B at 30 GHz measured by the radiometer at different beam positions over the land and sea: (upper panel) for 165° and 15° elevation angles; (middle panel) for 150° and 30° elevation angles; (bottom panel) for 135°, 90°, and 45° elevation angles. Each panel gives a direct comparison of T_B variation which is directly related to the evolution of clouds over sea and land.

by 17:30 LT, indicating the initiation of condensation of water vapor. However, the T_B over land during that time period remained low (∼100 K) until after 18:30 LT (for about one more hour) which further increased to ∼300 K at 19:00 LT, thus indicating that the convection reached at 15° beam position (over land) delayed by about 1.5 h from that observed over the sea (165°). As the convection progressed over the humid environment of the sea, the water-vapor density increased and the cooling of the updrafts provided enough supersaturation for rapid condensation on preexisting nuclei. Once condensation began, latent heat release supplemented the internal energy for a stronger updraft, resulting in more condensation and an increase in CLW and ice content. The upper panel of Fig. 5 shows the gradual increase in T_B over the sea (red line), which indicates the initial growth of convection. In the middle and bottom panels, the T_B variations over sea (red line) are very rapid, which indicates the presence of large amount of CLW content, further indicating that convection is in a mature stage. The green line in the bottom panel corresponds to the T_B variation at zenith. This multiangle elevation scan clearly shows the evolution of the convective system (in time) concurrent propagating horizontally from sea to land.

Fig. 5 also confirms the formation of a multicell, which can be thought of as a cluster of short-lived ordinary cells. Since these multicells are able to rebuild themselves constantly through new cell growth, they often last longer (hours) and cover a large area. After analyzing the waterspout observations for an 11-year period over the Western Mediterranean, Gaya *et al.* [8] concluded that in most of the cases the environment was not favorable for the supercell development. In the present case, waterspout has formed due to multicell cumulus clouds. In order to differentiate this multicell waterspout event from other convective events, we examined six cases (including the waterspout event day) that occurred in the month of April (2010, 2011). These convective events are intercompared in terms of increase in T_B at 22 GHz (ΔT_{B22}) (sensitive to water vapor) and 30 GHz (ΔT_{B30}), the vertical extent (H) of humidity (when RH ∼80%), and the duration (t) of the events. These analyses are summarized in Table I. The highest ΔT_B at both frequencies, for the waterspout event, indicates that it was the most intense among them with large amount of water vapor and liquid water up to higher altitude.

TABLE I
COMPARISON OF SIX CONVECTIVE EVENTS
(WATERSPOUT EVENT IS HIGHLIGHTED)

Date	4/4/10	5/8/10	**4/3/11**	4/17/11	4/23/11	4/28/11
$\triangle T_{B22}$	94.0	80.9	**118.2**	86.5	71.7	90.7
$\triangle T_{B30}$	189.1	185.1	**205.5**	188.0	182.3	186.5
H (km)	6-7	5	**9**	7	6	7-8
t (hrs)	3	4	**3**	6	2	5

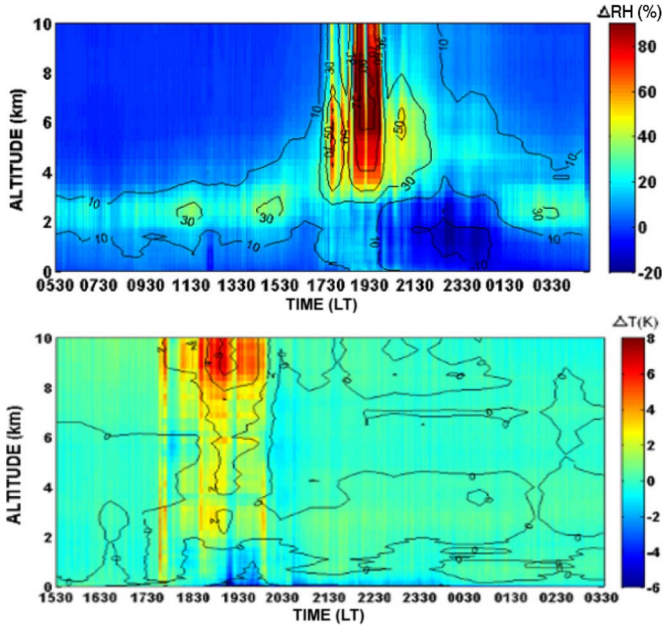

Fig. 6. (Upper panel) RH anomaly and (lower panel) temperature anomaly during the event day relative to the 10-day mean, with 5 days before and after the event day (excluding the event day).

IV. TEMPERATURE AND HUMIDITY ANOMALIES

To assess the variability in moisture and temperature during the event, the anomalies of these parameters were studied. The upper panel in Fig. 6 shows the RH anomaly estimated for the event day from 10-day mean (March 30 to April 10, sans April 3). A very large RH anomaly ($>$ 80%), is observed at altitudes above 4 km. Soon after the dissipation of convection, the humidity anomaly in the lower troposphere (below 3 km) drops to negative showing a dry atmosphere. This is further confirmed by the anomaly of absolute water-vapor content (WVD) (not shown here). The positive WVD anomaly (8 $g \cdot m^{-3}$) was observed at altitudes 4–6 km, and a negative anomaly of 2 $g \cdot m^{-3}$ persisted below 2 km.

The lower panel of Fig. 6 presents the temperature anomaly zoomed in for the convective period (15:30 to 03:30 LT), indicating a significant increase in temperature by 2–4 K at 2–6 km altitudes. As the convection grows, the moist air updrafts through the conditionally unstable atmosphere and undergoes condensation releasing large amount of latent heat energy, thus warming up the atmosphere. The nearly saturated downdraft, as it falls into the lower troposphere, mixes with the relatively dry air resulting in strong evaporational cooling. This cooling accelerates the downdraft (because of negative buoyancy), leading to the formation of a cold region in the lower portion of the convective cell close to the surface. Hence, a negative temperature anomaly of 2–4 K is observed in the lower troposphere below 2-km altitude. The convective vortices are more likely to form in the regions of warm and moist updrafts, and the cold and dry downdrafts are supported by the local environment [17]. The moisture- and temperature-anomaly analyses support this statement.

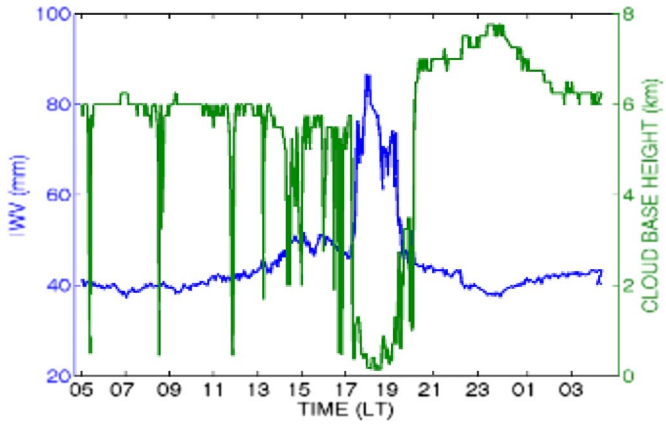

Fig. 7. Distribution of (left axis) IWV and (right axis) CBH during the convective event.

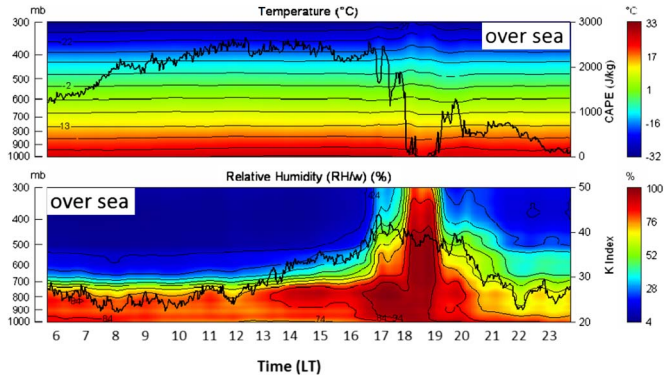

Fig. 8. Thick black lines represent CAPE in upper panel and K Index in lower panel, computed for the atmosphere over sea.

On the event day, the prevailing CBH was ∼6 km, but as the convection initiated, thick low clouds appeared and the CBH descended below 500 m (Fig. 7). Throughout the convective period (∼17:00 LT to ∼21:00 LT), the CBH remained below 1 km. Soon after the event, the CBH abruptly ascended above 8 km, as cirrus clouds were formed due to strong convective updraft. Fig. 7 also shows the background IWV, which was approximately 40 mm and suddenly increased up to 80 mm. In April, a typical wind pattern existed over TVM, with the onset of sea breeze at ∼09:00 LT and the land breeze at ∼19:00 LT, with maximum wind speed at ∼14:00 LT. Contrary to this conventional pattern, there was a sharp increase in wind speed from 0.5 m/s (prevailing condition) to above 2 m/s at ∼18:00 LT with a delay of ∼2 h in the onset of land breeze.

Thermodynamic instability (buoyancy) controls the vertical acceleration of air parcels while vertical wind shear influences the evolution of ordinary cells, multicells, or supercells. The convective available potential energy (CAPE) is an estimate of the updraft strength of a convective system. CAPE, estimated by integrating the potential temperature contributions along a representative parcel path, is shown in Fig. 8 along with K Index, which is an indicator of the occurrence of a thunderstorm, for the event day over the sea. The CAPE started building up at 07:00 LT from its prevailing value of ∼1300 $J \cdot kg^{-1}$ to

$\sim$2500 J $\cdot$ kg^{-1} by 12:00 LT and sustained for about 8 h which led to severe convection. Such a large CAPE can support the development of strong convective updrafts, downdrafts and cold pools, the latter being especially critical for the development of strong surface outflow. K Index was also high ($\sim$40) during the convective event. These forecast parameters also suggest that the conditions were conducive to strong convection.

A waterspout is an intense columnar vortex of small horizontal extent containing a funnel cloud of 5- to 100-m diameter with an average lifetime of 5–10 min suspended from a cumulonimbus cloud formed during the warm season when surface humidity and temperature are high. The cloudline scale is perhaps the most crucial for the waterspout formation, as at least 90% of the waterspouts are spawned by rapidly building cumulus cloud lines and not the isolated cumuli [18]. The continuous variations of RH and T_B shown in Figs. 4 and 5 correspond to the variations of CLW, which indicate the rapid and intense growth of cumuli and its longer persistence ($>$ 3 h) over the sea. These figures also show that the convective system grew to its maximum size (as it was seen in all the elevation angles simultaneously) before it rained and dissipated. The air temperature at the radiometer site was about 33 °C (maximum value), and the land-surface skin temperature was $\sim$50 °C. The monthly mean sea-surface temperature of April was $\sim$30 °C, and the monthly mean of IWV was $\sim$54 mm. These indicate a warm and humid atmospheric condition, with significant relative heating of land compare to sea, conducive to severe local convection and the formation of waterspouts once the instability in thermodynamics is established.

V. Conclusion

In this letter, results of the radiometric measurements in the microwave frequencies (K- and V-bands) of a tropical convective system which resulted in a waterspout over the coastal Arabian Sea are presented. The continuous evolution of humidity and temperature in the convective cloud system is retrieved from the radiometric observation. The changes in the microphysical cloud parameters and the energy exchange within the cloud system through the latent heat release are demonstrated. From these analyses, based on the radiometric T_B and the retrieved humidity and temperature profiles, we could observe the formation of multicell cumulus clouds over the warm coastal sea under the moist tropical conditions which were conducive to the development of a waterspout. During the convection, a warmer temperature anomaly was observed in the higher altitude ($>$ 4 km) which is associated with the strong updraft and condensation of water vapor by releasing the latent heat energy. The negative temperature anomaly of $\sim$2 K in the lower atmosphere ($<$ 2 km) is attributed to the cooling by downdraft of cooled dry air during the convection. The convective vortices, essential to the formation of waterspouts, are more likely to form in the regions of warm and moist updrafts, and the cold and dry downdrafts are supported by the local environment.

References

[1] B. Lin and W. B. Rossow, "Observation of cloud liquid water path over the oceans: Optical and microwave remote sensing methods," *J. Res.*, vol. 99, no. D10, pp. 20 907–20 927, 1994.

[2] C. Mätzler and J. Morland, "Refined physical retrieval of integrated water vapor and cloud liquid for microwave radiometer data," *IEEE Trans. Geosci. Remote Sens.*, vol. 47, no. 6, pp. 1585–1594, Jun. 2009.

[3] U. Löhnert, S. Crewell, and C. Simmer, "An integrated approach toward retrieving physically consistent profiles of temperature, humidity, cloud liquid water," *J. Appl. Meteorol.*, vol. 43, no. 9, pp. 1295–1307, Sep. 2004.

[4] J. Güldner and D. Spänkuch, "Remote sensing of the thermodynamic state of the atmospheric boundary layer by ground-based microwave radiometry," *J. Atmos. Ocean. Technol.*, vol. 18, no. 6, pp. 925–933, Jun. 2001.

[5] R. Ware, F. Solheim, R. Carpenter, J. Gueldner, J. Liljegren, T. Nehrkorn, and F. Vandenberghe, "A multi-channel radiometric profiler of temperature, humidity and cloud liquid," *Radio Sci.*, vol. 38, no. 4, pp. 8079–8092, 2003.

[6] J. Golden, "An assessment of waterspout frequencies along the United States East and Gulf Coasts," *J. Appl. Meteorol.*, vol. 16, no. 3, pp. 231–236, 1977.

[7] Y. Sugawara and F. Kobayashi, "Structure of a waterspout occurred over Tokyo Bay on May 31, 2007," *SOLA*, vol. 1, pp. 1–4, 2008.

[8] M. Gaya, V. Homar, R. Romero, and C. Ramis, "Tornadoes and waterspouts in the Balearic Islands: Phenomena and environment characterization," *Atmos. Res.*, vol. 56, no. 1, pp. 253–267, Jan. 2001.

[9] F. Solheim, J. Godwin, E. Westwater, Y. Han, S. Keihm, K. Marsh, and R. Ware, "Radiometric profiling of temperature, water vapor, cloud liquid water using various inversion methods," *Radio Sci.*, vol. 33, no. 2, pp. 393–404, 1998.

[10] J. C. Liljegren, S. A. Boukabara, K. Cady-Pereira, and S. Clough, "The effect of the half-width of the 22 GHz water vapor line on retrievals of temperature and water vapor profiles with a twelve-channel microwave radiometer," *IEEE Trans. Geosci. Remote Sens.*, vol. 43, no. 5, pp. 1102–1108, May 2005.

[11] R. Ware and D. Cimini, "Thermodynamic profiling at the Alpine Venue of the 2010 Winter Olympics," in *Proc. WMO Tech. Conf. Meteorol. Environ. Instrum. Methods Observ.*, Helsinki, Finland, 2010, pp. 1–6.

[12] R. S. W. Domenico Cimini and E. Campos, "Thermodynamic atmospheric profiling during the 2010 Winter Olympics using ground-based microwave radiometry," *IEEE Trans. Geosci. Remote Sens.*, vol. 49, no. 12, pp. 4959–4969, Dec. 2011.

[13] *WMO Guide to Meteorological Instruments*, WMO, Geneva, Switzerland, 20080, section II.5-4 5.2.4.

[14] E. R. Westwater, "Accuracy of water vapor and liquid determination by dual-frequency ground based microwave radiometry," *Radio Sci.*, vol. 13, no. 4, pp. 667–685, 1978.

[15] D. Cimini, T. J. Hewison, L. Martin, J. Güldner, C. Gaffard, and F. S. Marzano, "Temperature and humidity profile retrievals from ground-based microwave radiometers during TUC," *Meteorol. Zeitschrift*, vol. 15, no. 5, pp. 45–56, Feb. 2006.

[16] R. Ware and D. Cimini, "Ground-based microwave radiometer measurements during precipitation," in *Proc. 8th Spec. Meeting Microw. Radiometry*, Rome, Italy, Feb. 24–27, 2004, pp. 1–3.

[17] N. O. Renno, "A simple theory for waterspouts," *J. Atmos. Sci.*, vol. 58, no. 4, pp. 927–932, Apr. 2000.

[18] J. Golden, "The life-cycle of Florida keys waterspouts," *J. Appl. Meteorol.*, vol. 13, no. 6, pp. 676–692, Sep. 1974.